Section 1
PROGRESS IN LASER FUSION

1.A Phase Conversion Using Distributed Polarization Rotation

An essential requirement for direct-drive laser fusion is the uniform irradiation of fuel pellets located in the quasi far field of a multibeam laser system. To achieve the high-density compressions required for high-gain thermonuclear fusion, the implosion of the target fuel must be highly symmetric. More precisely, nonuniformities in the radiation pressure should not exceed 1% or 2%. To achieve this level of uniformity, not only accurate pointing, focusing, timing, and energy balance of the individual beams are required, but, more importantly, each of the laser beams must have a uniform focal-intensity distribution.

The intensity nonuniformities are caused by spatial variations in the near-field phase front of each laser beam.[1] Phase error, caused by variations in both geometrical path length and refractive index, is accumulated throughout each beamline. The frequency conversion of infrared light to ultraviolet light results in a tripling of beam phase error, causing larger intensity variations for ultraviolet light. This limits the level of irradiation uniformity that can be obtained by coherently focusing a laser beam. However, by modifying the phase or coherence properties of the laser beam, thereby changing its focusing characteristics, the level of irradiation uniformity can be improved. The method of induced spatial incoherence[2,3] (ISI) involves a reduction in both spatial and temporal coherence. Other approaches, such as random phase plates and lens arrays, are based on static spatial phase modulation of a laser beam.[4,5] The Laboratory for Laser Energetics has proposed a number of phase-conversion schemes, combining spatial phase

modulation with temporal phase modulation of a laser beam to demonstrate uniform, frequency-tripled laser radiation at the target plane.[6–9]

In the case of spatial phase conversion alone, the laser-plasma interaction physics is expected to differ from that with ideal target irradiation because of the stationary intensity fluctuations associated with a multibeamlet interference pattern. Generally, the short-wavelength interference structures that are 1% of the target diameter are assumed to be smoothed by thermal conduction in the plasma. However, it is currently unknown whether the detailed power spectrum of the phase-converted radiation, being shifted to shorter scale-length-intensity fluctuation, is more or less likely to "seed" the Rayleigh-Taylor hydrodynamic instability. Also, a high-intensity speckle in the laser can locally reduce the coronal plasma density, thereby increasing the refractive index and giving rise to self-focusing. The resulting breakup of the beam into self-focused filaments can then induce nonuniformities in the ablation pressure, as well as parametric instabilities.

Phase-conversion schemes involving broadband laser radiation, such as smoothing by spectral dispersion (SSD), can potentially reduce the likelihood of both filamentation and Rayleigh-Taylor instabilities, thereby providing the levels of irradiation uniformity required for ignition-scaling experiments. To improve the compression symmetry, the time interval for speckle shift must be short compared to the hydrodynamic response time of the plasma. High-peak-power Nd:glass lasers can, in principle, be operated with sufficient bandwidth to satisfy this requirement. However, the need for frequency tripling on OMEGA introduces certain constraints. For efficient frequency tripling, proper phase matching of broadband (~10-Å) light demands the use of infrared and ultraviolet diffraction gratings. Since large-aperture gratings of high damage threshold are not yet available, we are currently exploring alternative techniques designed to reduce the instantaneous level of irradiation nonuniformity on target.

One of the new phase-conversion techniques involves the use of beam-polarization segmentation, in conjunction with distributed phase plates (DPP's), such as those used on OMEGA. The effectiveness of this scheme has already been experimentally demonstrated by placing a half-wave retardation plate into half of a phase-converted laser beam. This resulted in significant reduction in speckle contrast over all spatial modes. More recently, a prototype distributed polarization rotator (DPR) has been fabricated and tested.[10] A time-instantaneous increase in irradiation uniformity has been likewise demonstrated using the DPR. In addition, by setting the polarization cycling to complement the color cycling produced by SSD, the time-dependent uniformity can be optimized.

In this article we first review the theory of speckle statistics, with which predictions of instantaneous speckle smoothing are obtained. Secondly, we describe the design of the DPR, highlighting the details of polarization, propagation, and interference. Lastly, we describe several experimental demonstrations, comparing them with the theoretical predictions.

Theory of Speckle Statistics

In general, phase conversion of laser light utilizes both spatial and temporal phase modulation to smooth the intensity distribution at the target plane. Schematically illustrated in Fig. 45.1, characteristics of the target-plane profile are determined by the size and distribution of elements within an optical array, such as a DPP. Time-varying phase and spatial phase modulation are used to smooth the resulting speckle distribution. The expression for two-beam interference is given by

$$I = I_1 + I_2 + [\boldsymbol{a}_1 \cdot \boldsymbol{a}_2]\,\mu_{12}(t)\,[I_1 I_2]^{1/2} \cos[(\omega_1 - \omega_2)t + (\phi_1 - \phi_2)], \quad (1)$$

where $\boldsymbol{a}$ is the polarization vector, I is the resulting intensity, ω is the angular frequency, and ϕ is the relative phase. Each of these parameters can be made to vary in space or time to smooth the interference pattern. Referring to Eq. (1), it is evident that incoherent addition of array elements is achieved when polarization vectors are orthogonal, causing the modulation term in the interference pattern to be zero and thus reducing the speckle contrast to zero. This is the basis for beam smoothing through polarization distribution. Correlation control between the spatial polarization segmentation, the DPP mask, and SSD color cycling provides additional smoothing mechanisms, but these mechanisms are not described in this article.

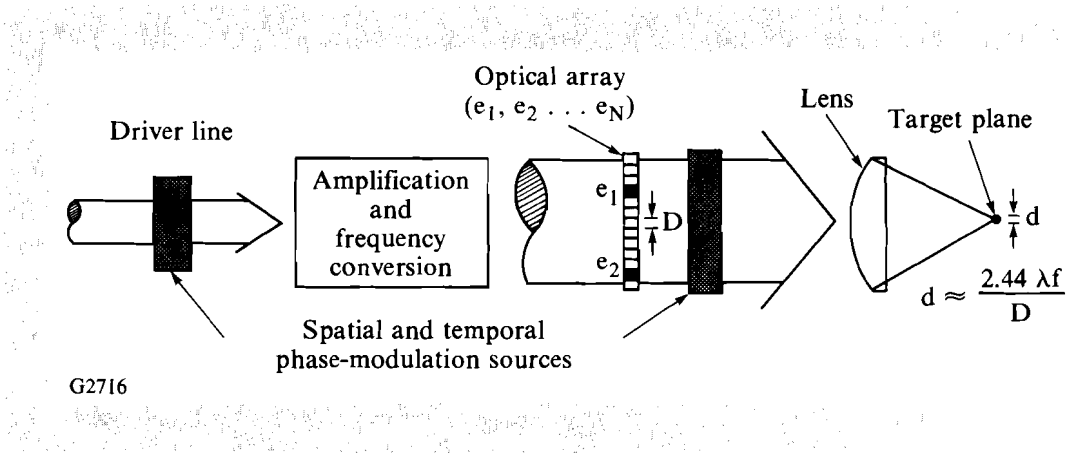

Fig. 45.1
Phase conversion of laser light, utilizing both spatial and temporal phase modulation, smooths the intensity distribution at the target plane. Spatial characteristics of the target-plane profiles are determined by an optical array placed before the focused lens; time-dependent phase, applied in the driver line, and additional spatial phase modulation, applied after frequency conversion, are used to smooth the resulting speckle distribution. Incoherent addition of array elements, instantaneously achieved when $\boldsymbol{a}_1 \cdot \boldsymbol{a}_2 = 0$ (i.e., $\boldsymbol{a}_1$, $\boldsymbol{a}_2$ are orthogonal), reduces speckle contrast.

A DPP is composed of an ordered array of transparent elements where the lateral dimension of each element is chosen to be small compared to the size of the phase and amplitude disturbances in the initial laser beam. Phase retardation is randomly distributed in an array of hexagons, each adding a phase delay of either 0 or π radians.

Collimated laser light transmitted through the DPP is broken into coherent, phase-retarded beamlets and brought to focus, where a superposition of beamlets is formed. Although the overlapped beamlets interfere to produce large intensity modulations at the target plane, with 10,000 beamlets per plate, the envelope of the focal distribution is a smooth distribution determined by the diffraction pattern of the individual area elements of the DPP and the detailed correlations between the DPP mask and the laser beam.

The amplitude distribution at the Fourier transform (focal) plane is given by

$$A(\varepsilon,\eta) = \int_{-\infty}^{\infty}\int a(\alpha_1,\beta_1)e^{-2\pi i(\alpha_1\varepsilon+\beta_1\eta)}\,d\alpha_1\,d\beta_1\,, \tag{2}$$

where $a(\alpha_1,\beta_1)$ is the complex amplitude distribution, $\varepsilon = \alpha_2/\lambda f$ and $\eta = \beta_2/\lambda f$ are the spatial-frequency variables, λ is the wavelength of light, and f is the focal length. The input amplitude is a product of the laser-beam amplitude (denoted by L) and the amplitude transmittance of the DPP.[6] The amplitude distribution $A(\varepsilon,\eta)$ can be conveniently expressed as

$$A(\varepsilon,\eta) \propto A_L(\varepsilon,\eta) \otimes \left[\frac{J_1(\pi d_o\omega)}{\pi d_o\omega}\right]\left[\sum_{j=1}^{N}\sum_{k=1}^{N} e^{2\pi i\left(\varepsilon\alpha_i+\eta\beta_K+\frac{\phi_{R_{j,k}}}{2\pi}\right)}\right]. \tag{3}$$

The random variable $\phi_{R_{j,k}}$ represents the phase retardation of the $(j,k)^{th}$ element (of size d_o).

The square of the envelope function $J_1(x)/x$, known as the Besinc function, where

$$\omega = \sqrt{\varepsilon^2+\eta^2}$$

represents the slowly varying profile of the focal intensity distribution $I(\varepsilon,\eta)$. The convolution in Eq. (3) (denoted by $\otimes$), between the far-field amplitude distribution of the laser beam $A_L(\varepsilon,\eta)$ and the product of a low-frequency envelope and a superposition of random spatial-frequency harmonics, is responsible for the detailed power spectrum of the resulting intensity distribution.

This intensity distribution is often referred to as laser speckle. Analysis of a speckle distribution can be performed using the classical model for random walk in the complex plane.[11] Using this approach, the statistical description of the amplitude distribution in Eq. (3) may be written as follows:

$$A(x,y,z) = \sum_{k=1}^{N}\frac{1}{\sqrt{N}}a_k(x,y,z) = \frac{1}{\sqrt{N}}\sum_{k=1}^{N}a_k e^{i\phi_k}\,, \tag{4}$$

where a_k and ϕ_k are assumed to be statistically independent for all k, and ϕ_k is uniformly distributed over $(-\pi,\pi)$.

Taking the limit of a large number of independent variables N and using the central limit theorem, it can be shown that the normalized probability-density function $P_1(I)$ of the intensity corresponding to one speckle pattern is given by

$$P_1(I) = \begin{cases} \frac{1}{\bar{I}} e^{-I/\bar{I}} & I \geq 0 \\ 0 & I < 0 \end{cases} , \tag{5}$$

where $\bar{I}$ is the average intensity.

The DPR, together with the DPP, produces two orthogonally polarized speckle patterns. The speckle patterns can be added on the basis of intensity since the modulation term of the interference pattern goes to zero as $\boldsymbol{a}_1 \cdot \boldsymbol{a}_2 = 0$. The normalized probability-density function $P_2(I)$ resulting from the intensity addition of two uncorrelated, but equally weighted, speckle patterns has also been derived in Ref. 11 and shown to be

$$P_2(I) = \frac{4I}{\bar{I}^2} e^{-2I/\bar{I}} . \tag{6}$$

The contrast associated with each speckle distribution, defined by

$$c \equiv \frac{\sqrt{\overline{I^2} - \bar{I}^2}}{\bar{I}} , \tag{7}$$

is found to be $\sqrt{2}$ smaller for the case of two speckle patterns added on the basis of intensity.

A simple explanation for the decrease in contrast can be given by examining the intensity probability-density curves plotted in Fig. 45.2. Curve P_1 shows that a limited number of high-intensity speckles are distributed within a large number of regions having zero intensity. The highest

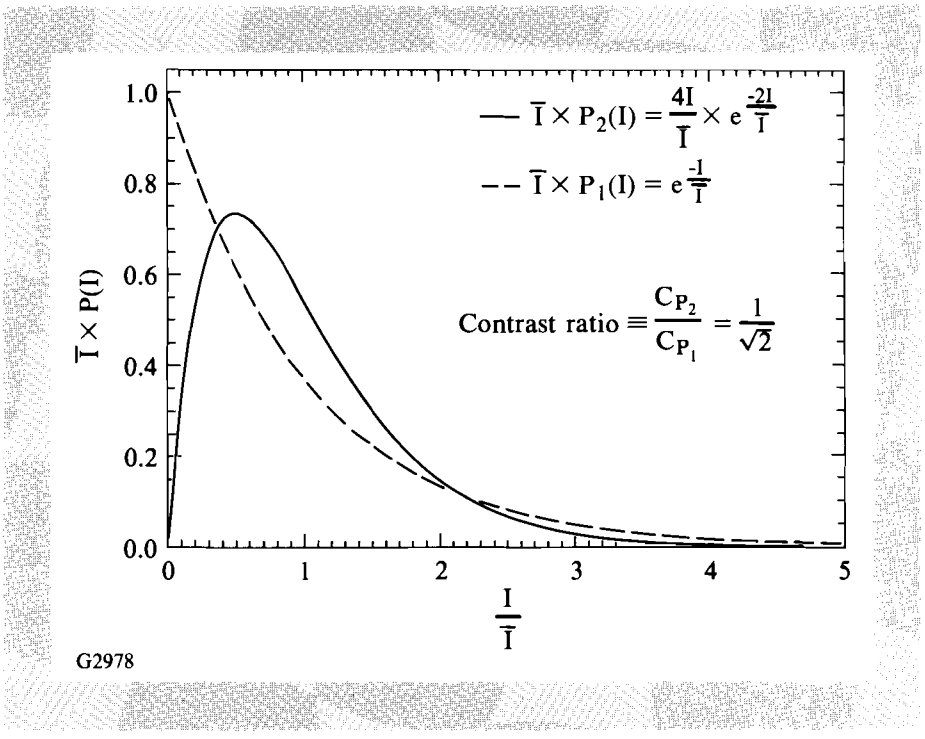

Fig. 45.2
The intensity probability-density function of one polarized, random speckle pattern obeys negative exponential statistics as shown in curve $P_1(I)$. Two speckle patterns, added on the basis of intensity, exhibit different intensity statistics as shown in curve $P_2(I)$. A greater number of intensity values falls near the mean intensity, the probability of higher intensity decreases, and the resulting speckle contrast is reduced by $\sqrt{2}$.

probability is for zero intensity. It is reasonable to expect that, for two uncorrelated distributions, the probability of exact overlap of the highest-intensity speckles is extremely low. Therefore, the number density of high-intensity speckles approximately doubles, the mean intensity doubles, but the value of the individual peaks remains the same. The probability-density function P_2, resulting from the incoherent addition of two speckle distributions, is also shown in Fig. 45.2. A decrease in speckle contrast is observed as an increase in the number of intensity values polling near the mean intensity. This decrease also applies to the addition of two orthogonally polarized and uncorrelated speckle patterns, since they effectively add on an incoherent basis. The greatest time-instantaneous improvement is obtained when the intensity peaks of one polarization fill the zeros of the orthogonal polarization at the transform plane. Correlation control of the phase mask can potentially optimize this effect for a particular DPR configuration.

Design of the DPR

The DPR is a wedged wave plate constructed from a birefringent fluid. As shown in Fig. 45.3(a), a nematic liquid-crystal fluid fills the volume within the wedge formed by two plane-parallel substrates. The birefringence varies linearly along the wedge as described by

$$\Gamma = t(y)\Delta n \ , \tag{8}$$

where Γ is the optical path difference between orthogonal polarizations, t is the path in the liquid crystal, and Δn is the birefringence of the fluid. The DPR transforms an incident linearly polarized beam into two orthogonally polarized beams. The incoming light is linearly polarized parallel to the DPR

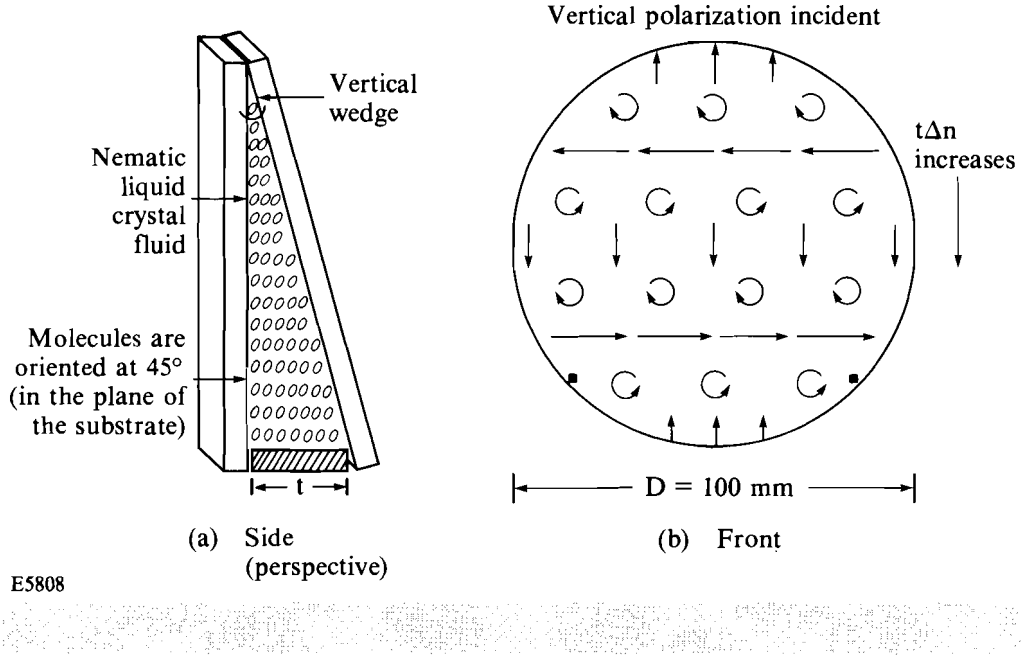

Fig. 45.3
The distributed polarization rotator (DPR) is an optical device that converts one polarized beam into two orthogonally polarized beams. The wedged DPR is a continuously varying wave plate that produces two co-propagating, orthogonally polarized, complementary interference patterns. A nematic liquid crystal fills a wedge formed between two parallel plates [Fig. 45.3(a)], yielding enough retardance to produce several polarization cycles along one dimension of the beam [Fig. 45.3(b)].

wedge angle. The fast and slow axes of the liquid crystal are oriented at ±45° to the wedge. The polarization of the transmitted light varies continuously for several cycles along the vertical dimension, as shown in Fig. 45.3(b).

Liquid-crystal DPR's are made in a manner similar to the fabrication of liquid-crystal polarizers and wave plates.[12] A polymer alignment layer is coated onto the inner surface of each substrate. This layer is unidirectionally rubbed at 45° with respect to the wedge angle formed by the two spacers [see Fig. 45.4(a)]. A 100-μm spacer is used to produce one milliradian of wedge. A nematic liquid crystal fills the wedge volume with the molecules anchored to the alignment layer, producing a molecular arrangement similar to that of a uniaxial crystal. The liquid-crystal fluid is a blend of saturated nematics, which are chosen to yield high-UV transmission and high damage threshold.[13] Figure 45.4(b) shows the molecular structure of the fluid and summarizes the performance criteria for which it was chosen as the optimum DPR material. The damage threshold of the saturated nematic blend surpasses requirements for both OMEGA and the proposed upgrade to OMEGA. Light transmission at $\lambda = 0.351$ μm is greater than 99% and is limited only by the quality of antireflection coating on the substrates and by the degree of index mismatch at the fluid-to-polymer and polymer-to-substrate interfaces.

Fig. 45.4
The DPR consists of two parallel plates, a polymer alignment layer and a thin layer of nematic liquid crystal [Fig. 45.4(a)]. The liquid-crystal molecules, anchored to a unidirectionally rubbed polymer film, exhibit uniaxial crystalline behavior. A blend of saturated nematics maximizes UV-laser-damage resistance and UV transmission. Liquid-crystal birefringence and the DPR wedge angle determine the polarization cycling rate illustrated in Fig. 45.3(b).

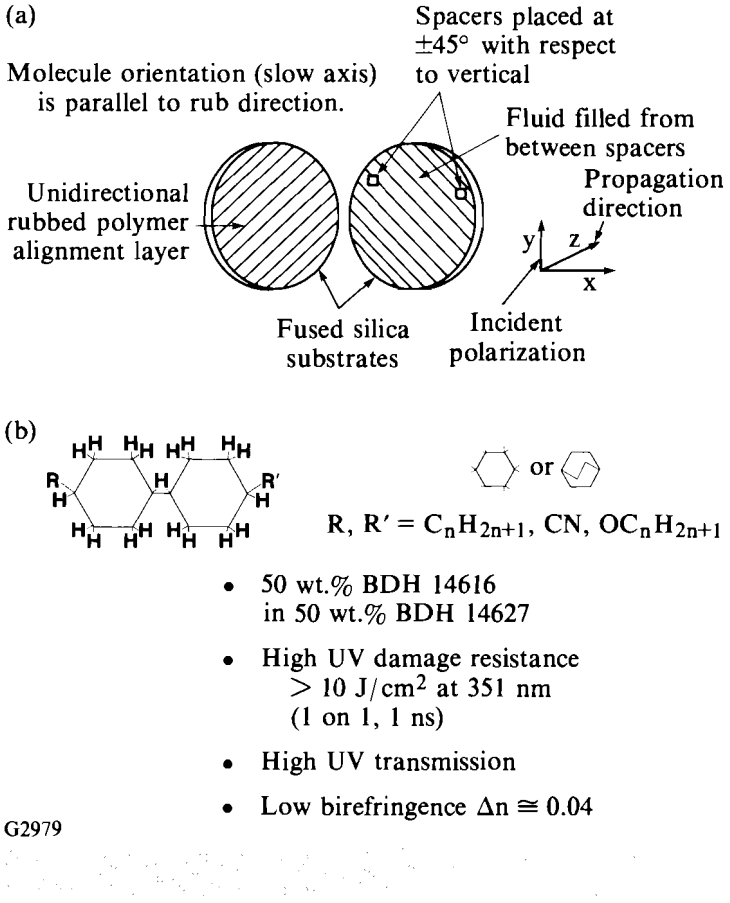

The wedged DPR is a continuously varying wave plate. The two polarizations produced are along the n_e and n_o axes (fast and slow axes, respectively) of the DPR. These directions are parallel and perpendicular to the rub direction or ±45° with respect to the wedge and the incident-light polarization. The ordinary and extraordinary components of the incident light experience unequal optical-path difference, again varying linearly in the vertical direction. These components of light experience a different wedge through the DPR and are tilted by a differential angle $\Delta\alpha_w$ given by

$$\Delta\alpha_w = \frac{t\Delta n}{D}, \tag{9}$$

where D is the DPR diameter, Δn is the birefringence, and t is the spacer thickness.

It is important that an angle exist between the two polarization components, since both components carry the same dephasing structure as they exit the DPP. Since each of these polarizations samples the whole phase plate, it is not correct to assume that the two speckle patterns are uncorrelated. In fact, they are strongly correlated but travel with different $\boldsymbol{k}$ vectors. This means that there exists a displacement between the two speckle fields. They are not registered exactly in space, but rather they are separated by a short correlation interval. Since this example does not satisfy the theoretical assumption of uncorrelated intensity addition, it is reasonable to expect that improvements in contrast would be greater for spatial frequencies closest in value to this correlation interval. Careful analysis of the speckle data is required. Results of such analysis are contained in the experimental section.

Another way of describing light transmitted through a DPR is based on polarization components that are parallel and perpendicular to the incident beam. In this case, the DPR is said to have produced two co-propagating, orthogonally polarized, complementary interference patterns. This perspective is completely consistent with the explanation involving angularly separated components since the grating angle is found to be equivalent to the differential-refraction angle as shown by

$$\theta_D = \lambda/d = \theta_R = d'/f, \tag{10}$$

where θ_D is the required grating angle of interference, θ_R is the differential-refraction angle (i.e., the angular separation of the two polarization components), d is the spacing of full-wave retardation or half-wave average phase delay, d' is the linear separation of the speckle pairs in the target plane, and f is the focal length of the targeting lens.

Experimental Demonstration

The DPR is placed within a two-dimensional, imaging, UV polariscope to demonstrate high-contrast polarization cycling. An argon-ion laser, operating at $\lambda = 351$ nm with vertical polarization, was used as the light source for the polariscope. One of two interference patterns transmits through the

analyzer to the imaging system as shown on the left side of Fig. 45.5. The vertical-line profile on the right shows high-contrast modulation, thus demonstrating high-polarization purity.

A far-field detection system images the light transmitted through the DPP and DPR (see Fig. 45.6). The profile at the left shows an intensity cross section from the DPP pattern, while the profile at the right shows an intensity cross section from the combination of a DPP and DPR. The azimuthal averages of the speckle profile show the characteristic envelope from the DPP hexagons. The contrast of speckle modulation is reduced by an amount greater than $\sqrt{2}$. This is seen by observing that the ratio of peak intensity to average intensity decreases with a DPR.

The individual intensity values of the measured speckle patterns are sorted to form the frequency function, referred to in the theory section as probability-density function. Referring to Fig. 45.7, the measured, non-DPR curve is shifted to the right of the theoretical, non-DPR curve. This is caused by a diagnostic limitation preventing correct measurement of intensity values near zero. Since this error is systematically present in all measurements, it is the ratio of speckle contrast that is important to assess the performance of the DPR. The measured contrast ratio with and without the DPR is greater than $\sqrt{2}$.

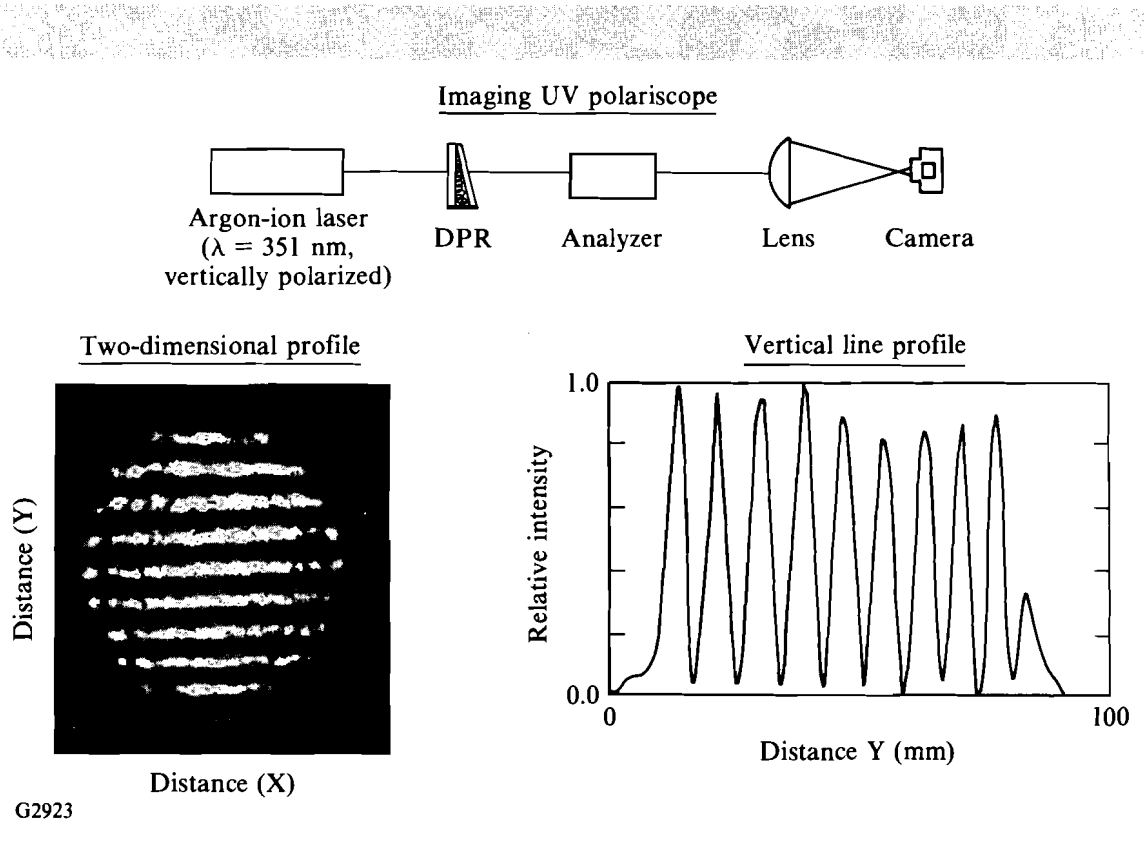

Fig. 45.5
The wedged DPR produces high-contrast, complementary interference patterns. The DPR is placed within a two-dimensional, imaging, ultraviolet polariscope to demonstrate high-contrast polarization cycling. One of two interference patterns transmits through the analyzer to the imaging system. The contrast of the sinusoidal intensity distribution, shown by the vertical line profile, is directly related to the purity of polarization cycling.

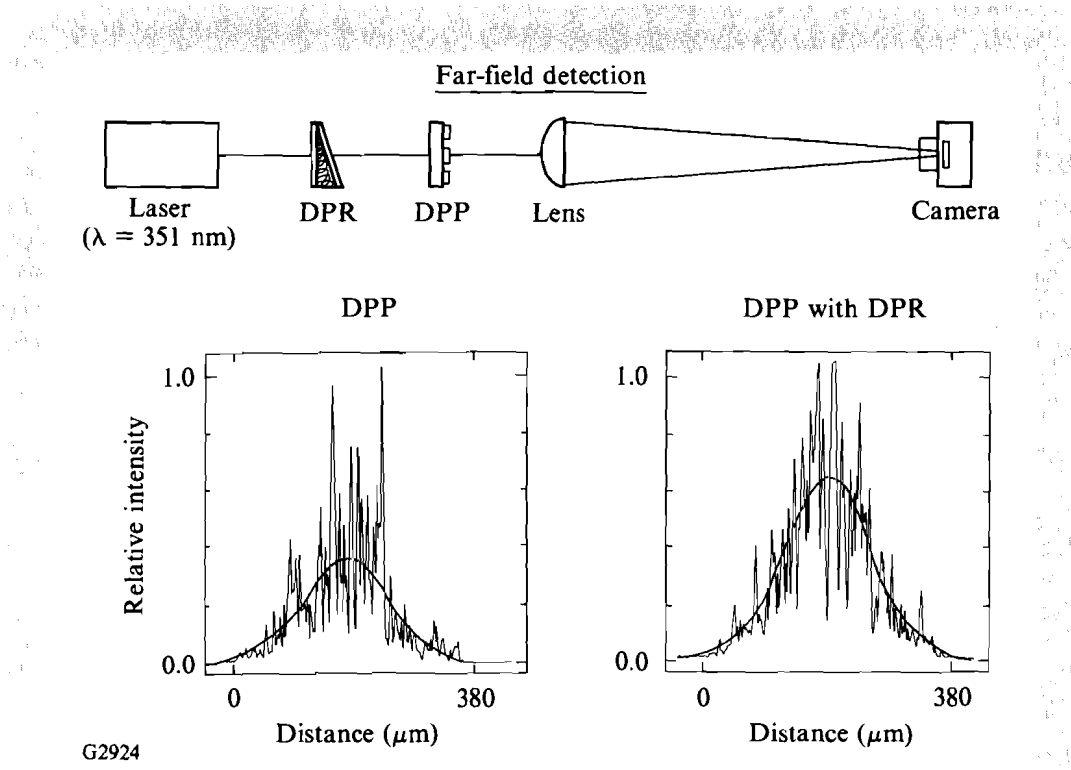

Fig. 45.6
The wedged DPR reduces the speckle intensity modulation in the far field of a DPP. The far-field detection system records the far-field image of the light transmitted through the DPP and DPR. The profile at the left shows an intensity cross section from the DPP pattern. The profile at the right shows an intensity cross section from the combination of a DPP and a DPR. The speckle modulation is reduced by more than $\sqrt{2}$. This is seen by observing that the ratio of peak intensity to average intensity decreases with a DPR.

Time-integrated, equivalent-target-plane focal spots of the combination of broadband phase conversion and distributed polarization rotation have recently been generated on one beam of the OMEGA laser system. Improvements in light uniformity are difficult to diagnose due to the time-integrated effects of SSD and the results do not fully reflect the time-instantaneous benefit. The case in which the polarization cycling and the color cycling are orthogonal shows improvement in uniformity as compared to the case in which they are both parallel. It has been calculated that, by orienting the polarization cycling orthogonal to the direction of color cycling from SSD, a reduction from 4.0% to 2.8% in the time-integrated nonuniformity can be achieved.

It is anticipated that an additional benefit of polarization segmentation may be realized if the DPR is placed well in advance of the DPP. Beam deflection occurs outside the image plane of the source of angular dispersion, i.e., the diffraction grating. By placing the DPR well in advance of the DPP,

the angular dispersion between the elements would produce a spatial deflection that results in a time-varying polarization that samples the individual elements of the DPP. Therefore, if the polarization cycling frequency is high enough to fully sample different elements on the DPP, then an additional source of beam smoothing is expected to contribute to time-dependent uniformity improvements.

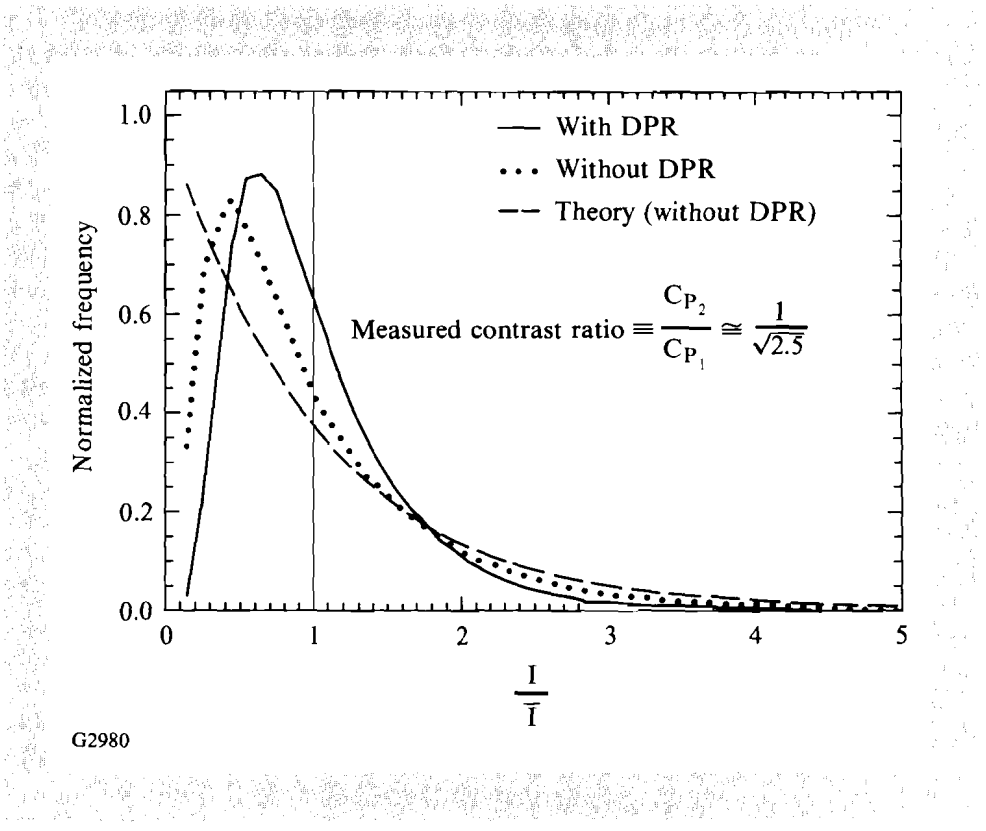

Fig. 45.7
Time-instantaneous decrease in speckle contrast, produced by the DPR, is measured to be greater than $\sqrt{2}$. Assessment of the full benefit of the DPR is currently diagnostic limited, as seen by comparing theoretical and experimental curves for the case with a DPR.

Summary

An essential requirement of direct-drive inertial confinement fusion is the uniform irradiation of spherical targets placed in the quasi far field of a laser beam. Phase-conversion technologies continue to provide the OMEGA laser system with substantially improved levels of irradiation uniformity for targets placed close to the far-field plane. Furthermore, the relevant phase-conversion technologies are flexible and inexpensive.

A new phase-conversion technique based on a DPR has been developed to provide smoothing of the laser intensity on target. It has been shown theoretically and experimentally that one-dimensional DPR reduces the contrast of speckle nonuniformities by a factor of $\sqrt{2}$. This technique instantaneously achieves a level of uniformity that current time-domain techniques, such as SSD, require tens of picoseconds to achieve, assuming a time-integrated response from the target. It is expected that a combination of all phase-conversion techniques will provide levels of irradiation uniformity necessary for future direct-drive laser-fusion research.